

Structural, optical, magnetic, and electrical properties of nanospinels containing different molar ratios of cobalt and aluminum ions

**Emad M. Masoud, A.-A. El-Bellihi,
W. A. Bayoumy & Eman S. Abdelazeem**

Ionics

International Journal of Ionics The
Science and Technology of Ionic Motion

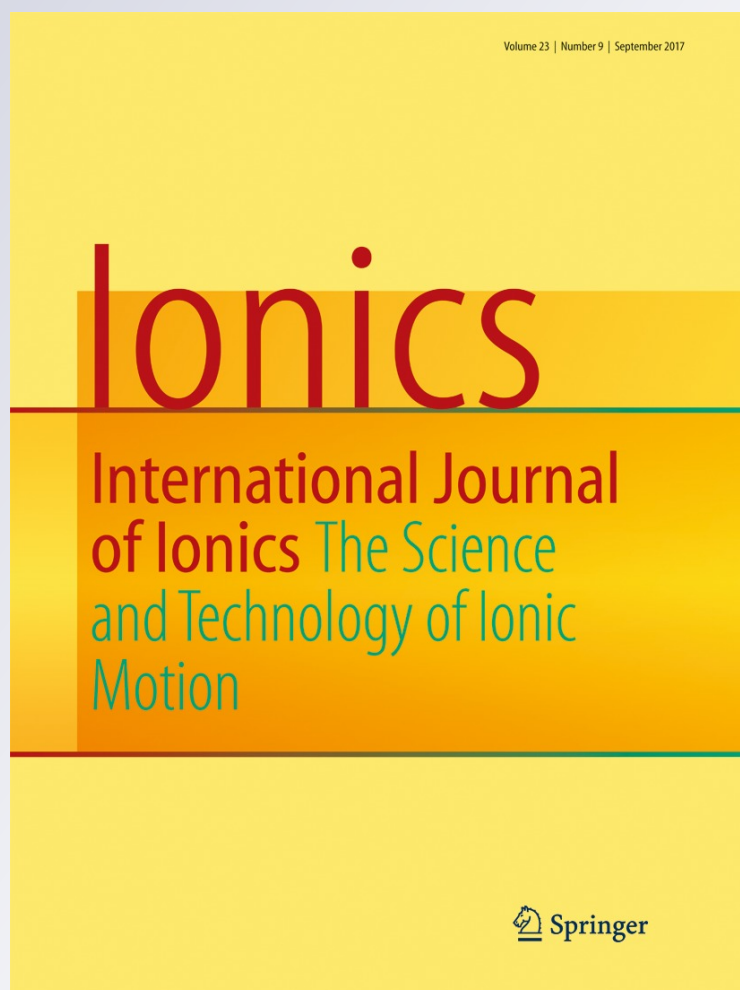
ISSN 0947-7047

Volume 23

Number 9

Ionics (2017) 23:2417-2427

DOI 10.1007/s11581-017-2091-0



Your article is protected by copyright and all rights are held exclusively by Springer-Verlag Berlin Heidelberg. This e-offprint is for personal use only and shall not be self-archived in electronic repositories. If you wish to self-archive your article, please use the accepted manuscript version for posting on your own website. You may further deposit the accepted manuscript version in any repository, provided it is only made publicly available 12 months after official publication or later and provided acknowledgement is given to the original source of publication and a link is inserted to the published article on Springer's website. The link must be accompanied by the following text: "The final publication is available at link.springer.com".

Structural, optical, magnetic, and electrical properties of nanospinels containing different molar ratios of cobalt and aluminum ions

 Emad M. Masoud¹ · A.-A. El-Bellihi¹ · W. A. Bayoumy¹ · Eman S. Abdelazeem¹

 Received: 8 January 2017 / Revised: 24 March 2017 / Accepted: 26 March 2017 / Published online: 14 April 2017
 © Springer-Verlag Berlin Heidelberg 2017

Abstract Aluminum substituted by cobalt of cobalt aluminates having a nominal composition $\text{CoCo}_x\text{Al}_{2-x}\text{O}_4$, where $x = 0, 0.5, 1, 1.5,$ and 2 , were synthesized by the thermal decomposition of complex precursors derived from metal nitrate salts and glycine. All samples were characterized using different techniques, XRD, FT-IR, TG, DTA, DSC, and TEM. XRD showed that all samples have a spinel cubic crystal structure. Using Debye–Scherrer formula, the calculated crystallite size was found cobalt concentration dependent and varied between 21 and 32 nm. Lattice parameter, X-ray density, porosity, and unit cell volume were calculated to show the effect of Al^{3+} substitution by cobalt on the crystal structure of the investigated spinel samples. Cation distribution and oxygen content into specific spinel stoichiometry of all samples were calculated. The optical, magnetic, and electrical properties were also studied. The spinel nano cobalt aluminate ($x = 0.5$) having Co/Al molar ratio of 1 showed the highest values of saturation magnetization ($M_s = 1.1 \text{ emu g}^{-1}$) and conductivity ($3.1 \times 10^{-8} \Omega^{-1} \text{ cm}^{-1}$) compared to the other ones. The color parameters (L^*, a^*, b^*) were also measured. All results were collected and discussed.

Keywords Nano cobalt aluminate · High saturation magnetization · Electrical properties

Introduction

The synthesis of nanocrystalline spinel using different methods [1–7] has been investigated intensively due to the unique potential applications such as high-density magnetic recording and microwave devices, as magnetic fluids, and also as an absorbent material to remove sulfide gases from hot coal gas [8, 9]. The general formula of spinels is AB_2O_4 . In the spinel structure, the anions are arranged in a cubic close-packed array with the cations arranged in the holes of the array. There are eight tetrahedral and four octahedral holes per molecule. In the case of normal spinels, the A^{2+} ions occupy tetrahedral holes and B^{3+} ions are present in the octahedral holes. In the case of inverse spinels, one half of A^{2+} ions occupy tetrahedral holes and the remainder of A^{2+} ions and all B^{3+} ions occupy the octahedral holes [10]. It is known that the nature of occupancy of tetrahedral and octahedral sites depends on the calcination temperature [11]. One example is the cobalt aluminate material system from which a series of $\text{Co}^{\text{II}}\text{Co}^{\text{III}}_x\text{Al}_{2-x}\text{O}_4$ spinels (where $x = 0–2$) can be derived [12–16], including CoAl_2O_4 , Co_2AlO_4 , Co_3O_4 , etc. CoAl_2O_4 is well known as Thenard's blue for its impressive optical property and widely used in the ceramics, glass, paint industry, and color TV tubes as contrast-enhancing luminescent pigment [17]. The common methods reported for the synthesis of cobalt aluminate are sol–gel [18], EDTA chelating precursor [19], combustion [20, 21], polymerized complex [22], glycine chelated precursor [23], hydrothermal [24], molten salt [25], polymer aerosol pyrolysis [26], and reverse micelle processes [27, 28]. Many researchers tried to enhance the cobalt aluminate properties depending on the particle size methodology that can be controlled in nanosize using the different above methods. Doping in aluminates was also one of the methodologies. As we all know, the substitution of Al^{3+} ions by cobalt ones' process can have an effect on all the

✉ Emad M. Masoud
 emad.youssef@fsc.bu.edu.eg; emad_masoud1981@yahoo.com

¹ Department of Chemistry, Faculty of Science, Benha University, 13518 Benha, Egypt

properties of the material such as the magnetic one as cobalt ions have very good magnetic moments compared to aluminum ones. Moreover, the presence site (tetrahedral or octahedral) of cobalt ions as well as their oxidation states (divalent or trivalent) in the spinel structure will affect the energetic structure stability and as a result leading to a definite spin configuration that will determine its magnetic moment behavior.

In this vein and as an example, Co consistently favors a low spin configuration with no significant magnetic moment when placed on an octahedral site. However, when Al occupies the tetrahedral sites in the less stable normal Co_2AlO_4 and inverse CoAl_2O_4 structures, Co is forced into a d^7 configuration producing a magnetic moment of almost $3 \mu_B$ [29].

Additionally, factors such as electronic band gap and charge distribution can affect more on the electrical properties of spinels as the conduction process depends mainly on hopping of charge on octahedral sites. Thus, the presence of different valence states among octahedral cations is essential.

To the best of our knowledge, none of these works have been devoted to study the effect of molar ratio (Co/Al) change in the cobalt aluminate spinel, without the doping methodology, on the different properties of CoAl_2O_4 . Here, for the first time, we try to investigate the structural, magnetic, optical, and electrical properties of spinel cobalt aluminate prepared using different molar ratios of cobalt/aluminum (Al^{3+} substitution by Co^{2+} or Co^{3+}), without a dopant, and depending on the ability of cobalt ion to occupy the positions of aluminum in the octahedral sites to compensate the lack of aluminum to form the cubic spinel structure.

Experimental

Synthesis of nano spinels (cobalt aluminates and cobalt oxide)

$\text{Co}(\text{NO}_3)_2 \cdot 6\text{H}_2\text{O}$ (>98%, Fluka), $\text{Al}(\text{NO}_3)_3 \cdot 9\text{H}_2\text{O}$ (>98.5%, Merck), and glycine (>99.7%, Merck) were used as received without further purification. Appropriate amounts of the starting materials were used (Table 1) to prepare different molar ratios of Co/Al = 0.5, 1, 2, and 5, in addition to a free aluminum sample denoted as FAS according to the following

Table 1 Appropriate amounts of $\text{Co}(\text{NO}_3)_2$, $\text{Al}(\text{NO}_3)_3$, and glycine used for different molar ratios (Co/Al) preparations

Molar ratio, Co/Al	$\text{Co}(\text{NO}_3)_2$ (mol)	$\text{Al}(\text{NO}_3)_3$ (mol)	Glycine (mol)
0.5	0.010	0.020	0.044
1	0.150	0.150	0.042
2	0.020	0.010	0.039
5	0.025	0.005	0.036
FAS, Co_3O_4	0.030	zero	0.033

formula, $\text{CoCo}_x\text{Al}_{2-x}\text{O}_4$, where $x = 0, 0.5, 1, 1.5$, and 2, to form the following structures: CoAl_2O_4 , $\text{CoCo}_{0.5}\text{Al}_{1.5}\text{O}_4$, Co_2AlO_4 , $\text{Co}_2\text{Co}_{0.5}\text{Al}_{0.5}\text{O}_4$, and Co_3O_4 , respectively).

All starting materials were introduced with a magnetic stirring into 36 ml distilled water. Two kinds of chelated complexes formed with the dissolution of the nitrate salts in the solution. A deep purple solution was obtained and further heated at 70°C overnight to remove excess water. During a continuous heating, the solution became more and more viscous and finally became a xerogel. The resulting highly viscous xerogel was calcined at 600°C (at a rate of about $10^\circ\text{C min}^{-1}$) for 3 h to finally get green cobalt aluminates and cobalt oxide samples.

Characterization of samples

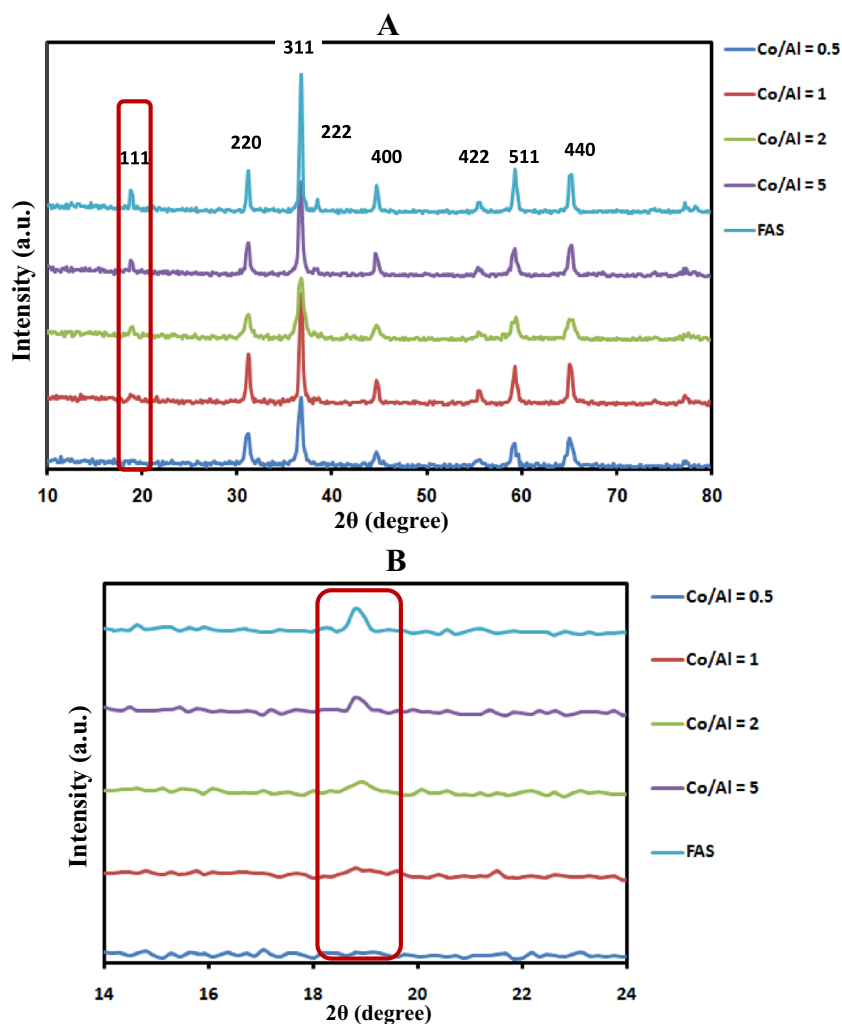
X-ray diffraction analysis was performed on a Diano (made by Diano Corporation, USA). The pattern was run with Cu-filtered $\text{CuK}\alpha$ radiation ($\lambda = 1.5418 \text{ \AA}$) energized at 45 kV and 10 mA. The samples were measured at room temperature in the range from $2\theta = 10^\circ$ to 80° . The infrared spectra of the samples were recorded in the range of $4000\text{--}400 \text{ cm}^{-1}$ using a Bruker FT-IR. TG, DTA, and DSC were performed in nitrogen atmosphere with a constant heating rate of 10 K min^{-1} in a temperature range of 298–1273 K using Shimadzu DT-50.

The electrical conductivity measurements were performed by sandwiching the powder samples (tablets) between two stainless steel electrodes using a programmable automatic LCR bridge (Model RM 6306 Phillips Bridge) in various temperatures ranging from 298 to 388 K. The UV-vis spectra were recorded on a UV-visible spectrophotometer (Jasco, model v670). The magnetic properties were measured using vibrating sample magnetometer (VSM; Lake Shore 7404). The morphology was analyzed using transmission electron microscope (TEM) operating at an accelerating voltage of 200 kV (JEOL, JEM 2100F).

Results and discussion

The XRD patterns of the samples are shown in Fig. 1a. The observed diffraction peaks correspond to the standard patterns of the spinel (ICSD 01-082-2251). By a close inspection for all patterns, one can notice an important indication for the presence of Co^{3+} and Co^{2+} in all spinel structures (except for the sample containing Co/Al = 0.5, containing Co^{2+} ions only), the small peak (111) at 16° that is characteristic to Co_3O_4 spinel phase. To confirm this aspect in an obvious shape, partially enlarged drawing peak (111) is shown in Fig. 1b. The figure showed that this peak intensity arises with Co/Al molar ratio. This confirms that the Co^{3+} ion ratio increases upon the increase of Co/Al molar ratio to reach maximum for the FAS sample. No other crystalline phases (like oxides of aluminum) appear in the samples, confirming the tendency

Fig. 1 X-ray diffraction patterns of (a) spinel cobalt aluminate structures containing different Co/Al molar ratios and (b) partially enlarged drawing of spinel structure peak (111)



of cobalt ions to compensate the lack of aluminum ions (Al^{3+}) in the octahedral sites of the spinels that can be fully occupied only by cobalt ions in FAS to form the investigated spinel structures, CoAl_2O_4 , $\text{CoCo}_{0.5}\text{Al}_{1.5}\text{O}_4$, Co_2AlO_4 , $\text{Co}_2\text{Co}_{0.5}\text{Al}_{0.5}\text{O}_4$, and Co_3O_4 with the following molar ratios, Co/Al = 0.5, 1, 2, 5, and FAS, respectively. Extremely broad peaks are observed, and those indicate the presence of very fine particles. The crystallite size of the samples obtained using Scherrer equation [30] was found in a range of 21–32 nm.

Figure 2 shows the FT-IR spectra of nanospinels. The band at 3470 cm^{-1} is attributed to the stretching vibrations of the hydrogen-bonded OH groups [31]. The absorption band at 2964 cm^{-1} is related to C–H stretching vibration from the organic compound (glycine) [31]. The characteristic stretching bands between 1590 and 1720 cm^{-1} are due to –COOH stretching vibrations [32, 33]. The absorption band at 1097 cm^{-1} is probably due to CH–OH stretching vibration [32]. The bands over the range of 1000 – 400 cm^{-1} ($662, 570\text{ cm}^{-1}$) correspond to metal–oxygen bond (Co–O

and Al–O stretching) vibrations for the spinel structure compound [31] that is already confirmed by XRD (Fig. 1). The

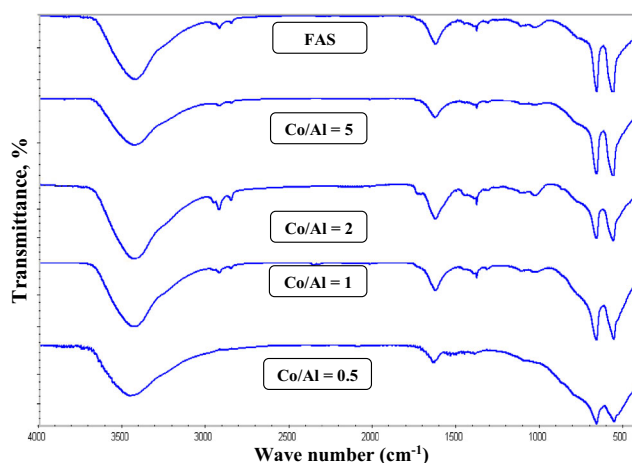


Fig. 2 FT-IR spectra of spinel cobalt aluminate structures containing different Co/Al molar ratios

presence of –OH group in the sample is possibly due to the moisture absorption.

To investigate the percent of glycine complexes formed with the spinel structures and to know the stability of these complexes with different molar ratios (Co/Al) of spinels, the thermochemical behavior of nanospinels (0.5, 2, FAS) is shown in Fig. 3a, b, c. The figures show that there is a weight

loss till a temperature of 1000 °C for the first two samples (a, b) and till 870 °C for c sample. The decrease of weight till 300 °C corresponds to the volatilization of free and adsorbed water molecules existing in the samples. In the temperature region between 300 and 1000 °C, the weight loss is caused by the decomposition of Co–Al glycine complex traces in the sample, confirmed by FT-IR (Fig. 2). Above 1000 °C, the

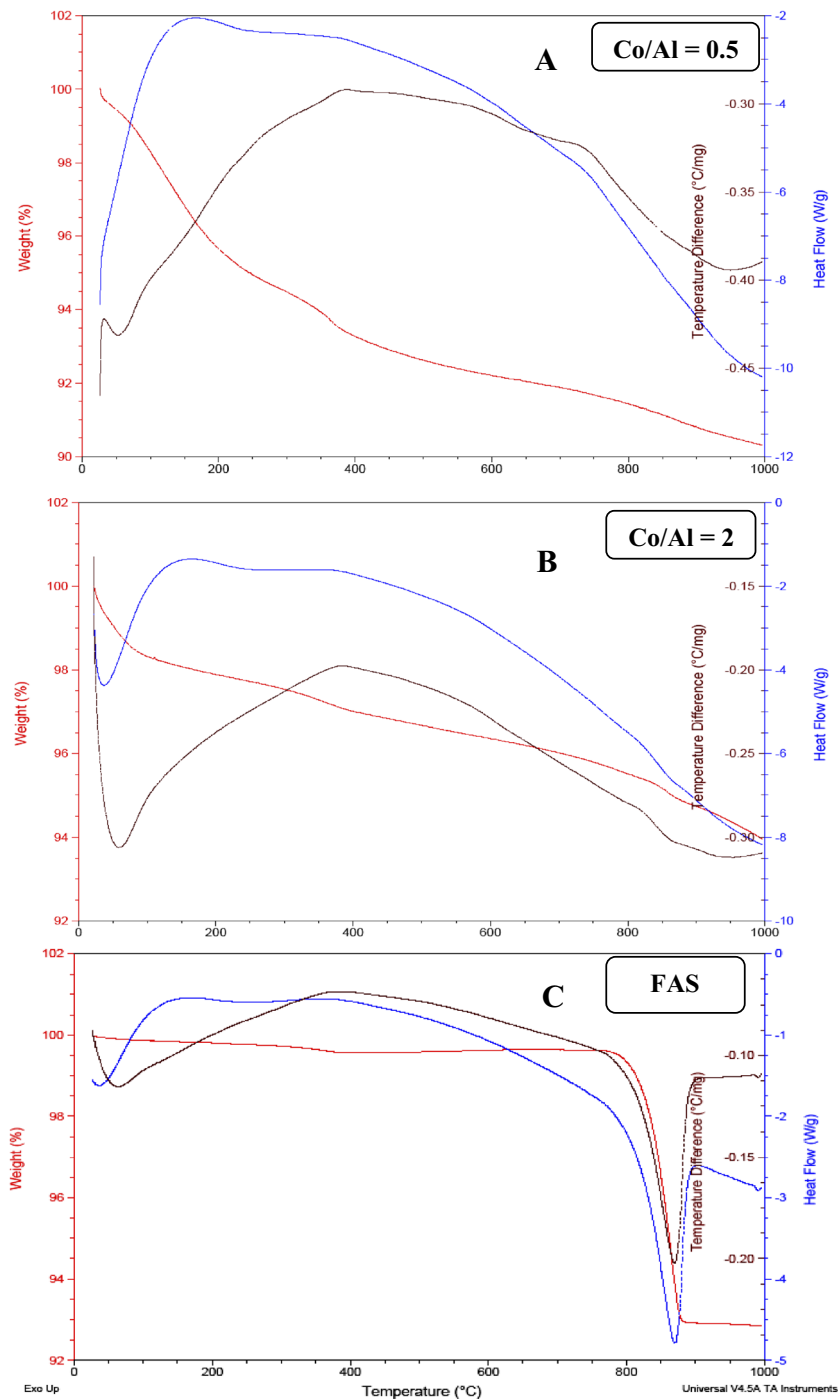


Fig. 3 Thermal analysis (TG, DTA, DSC) patterns of spinel cobalt aluminate structures containing different Co/Al molar ratios. **a** Co/Al = 0.5. **b** Co/Al = 2. **c** FAS

weight of the sample is constant, which indicates the completion of decomposition and the formation of pure spinels. The Co–Al glycine complex traces can be determined as 3 wt% for samples a and b and 7 wt% for c. The thermal decomposition behavior is associated with the endothermic and exothermic effects. The first region weight loss due to the removal of adsorbed water is indicated by two small endothermic peaks between 60 and 300 °C in the DTA curve. An exothermic peak at around 400 °C is due to the decomposition of Co–Al glycine complex traces. More notably, the weight starts to be stable at 1000 °C for a and b samples, but at 870 °C for c one. This can show that glycine complexes have a different thermal stability with the different molar ratio of spinel structures, where the FAS, c, showed more glycine complex thermal stable behavior compared to a and b samples.

For structure investigation, lattice parameter (*a*), unit cell volume (*V*), X-ray density (*d_x*), bulk density (*d_b*), and porosity parameters were calculated and shown in Table 2. The value of lattice parameter (*a*) of the Co/Al = 0.5 as calculated from XRD data ($a = d_{hkl} (h^2 + k^2 + L^2)^{1/2}$) is 8.101 Å. The lattice parameter increases on increasing the molar ratio (Co/Al) to have a value of 8.129 for FAS, Co₃O₄ spinel structure, as shown in Fig. 4a. The increase in lattice parameter is due to the fact that the ionic radius of Co²⁺ or Co³⁺ (i.e., 0.745 or 0.61 Å) is larger than that of Al³⁺ (0.535 Å) [34]. Also, the increase of lattice parameter on increasing the concentration of cobalt ions demonstrates that the Co ions actually compensate the lack of Al³⁺ ion concentration and occupy the octahedral sites for all spinel samples [35]. The X-ray density for all samples was calculated using the relation [36] $d_{x-ray} = Z \times M / N_A \times V_{cell}$, where *Z* is the number of molecules per formula unit (8 for the cubic structure), *M* is the molar mass, *N_A* is the Avogadro's number ($6.02 \times 10^{23} \text{ mol}^{-1}$), and *V_{cell}* is the unit cell volume (*a*³). The bulk density was calculated by the following equation [37]:

$d_{bulk} = m / V$ where *m* is the mass and $V(\pi r^2 h)$, where *r* is the radius and *h* is the height/thickness of pellet) is the volume of the pellet. The percentage porosity of all samples was calculated using the relation [38]:

$P = 1 - d_b/d_x$ where *d_b* is the bulk density and *d_x* is the X-ray density. Figure 4b shows that the *d_x* increases on

Table 2 Lattice parameter (*a*), unit cell volume (*V*), X-ray density (*d_x*), bulk density (*d_b*), and porosity of spinel cobalt aluminate structures containing different molar ratios (Co/Al)

Molar ratio, Co/Al	<i>a</i> (Å)	<i>V</i> (Å ³)	<i>d_x</i> (g cm ⁻³)	<i>d_b</i> (g cm ⁻³)	Porosity (%)
0.5	8.101	531	4.42	1.4941	66
1	8.104	532	4.81	1.9340	60
2	8.120	535	5.18	2.2570	56
5	8.124	536	5.57	3.1811	43
FAS, Co ₃ O ₄	8.129	537	5.96	3.4296	42

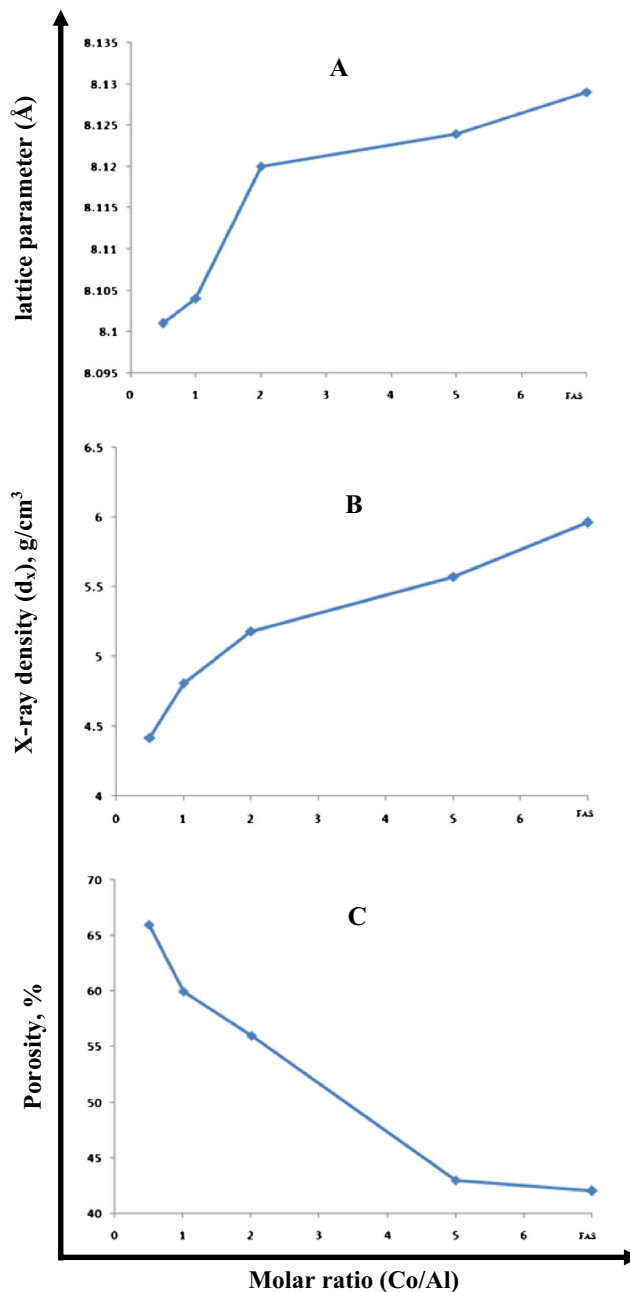


Fig. 4 Molar ratio dependence of **a** lattice parameter, **b** X-ray density, and **c** porosity for spinel cobalt aluminate structures containing different Co/Al molar ratios

increasing cobalt concentration of spinels to have a value of 5.96 g cm⁻³ for FAS, Co₃O₄ spinel structure. The increase in the *d_x* is considered to be due to the fact that the atomic mass of cobalt (59 amu) is larger than that of aluminum (26.98 amu) [38]. While the increase in the *d_b* (Table 2) is due to the fact that cobalt (8.90 g cm⁻³) has larger value of density as compared to that of aluminum (2.702 g cm⁻³), the magnitude of the *d_b* is smaller than that of the *d_x* as can be seen in Table 2. These results indicate that the experimental *d_b* is less than the theoretical *d_x*, and this can be attributed to the presence of pores created during sintering

Table 3 Structural data of spinel cobalt aluminate structures containing different molar ratios (Co/Al)

Molar ratio, Co/Al	a_{th} (Å)	a (Å) _{exp.}	r_A (Å)	r_B (Å)	Tetrahedral		Octahedral	
					Co	Al	Co	Al
0.5	8.104	8.101	0.6250	0.5949	0.4977	0.5022	0.5022	1.4977
1	8.055	8.104	0.6208	0.5833	0.7436	0.2564	0.7564	1.2436
2	8.082	8.120	0.5366	0.6391	0.9996	0.0003	1.0003	0.9996
5	8.124	8.124	0.5582	0.6421	0.8520	0.1480	1.6480	0.3520
FAS, Co ₃ O ₄	8.155	8.129	0.5350	0.6675	1	0	2	0

process [39]. As shown in Fig. 4c, the porosity decreases with the increase of molar ratio (Co/Al) to have a value of 42% for FAS, Co₃O₄ spinel structure. This is because of the increase in the X-ray density (d_x). The increase in the d_b verifies that samples become denser with cobalt concentration increase.

To further investigate the presence of both aluminum and cobalt in both tetrahedral and octahedral arrangements of the spinels, the radii of the tetrahedral (r_A) and octahedral (r_B) sites and also the theoretical lattice parameter (a_{th}) were calculated [40] (Table 3). The theoretical lattice parameter values come in a good agreement with the experimentally one, leading to an appropriate cation distribution reported in Table 3. The table data showed and approved our main manuscript idea, the ability of cobalt ions to compensate the lack of aluminum ones in the octahedral sites to form the different spinel structures. Also, the octahedral cobalt content (Co²⁺ for the Co/Al = 0.5 sample and Co²⁺ and Co³⁺ for the other ones) increases gradually to equal 2 in the FAS sample. Another interesting phenomenon, which can give us an indication for the predominant octahedral cobalt content (Co²⁺ or Co³⁺), is the oxygen content into spinel-specific stoichiometry of the cobalt aluminate spinel samples. The values of oxygen content ratio were calculated from X-ray photon spectroscopy (XPS) and reported in Table 4. In general, the lack of oxygen content ratio may lead to a presence of a predominant octahedral Co²⁺ content in the spinel structure, and a predominant octahedral Co³⁺ content is achieved when there is oxygen content ratio increase. So, according to the table of oxygen content ratio, the samples of Co/Al = 1 and 5 contain a predominant of Co³⁺, but the samples of Co/Al = 2 and FAS contain a predominant of Co²⁺.

Table 4 Oxygen content into specific spinel stoichiometry (calculated from X-ray photon spectroscopy (XPS)) of spinel cobalt aluminate structures containing different molar ratios (Co/Al)

Molar ratio, Co/Al	Oxygen content into specific spinel stoichiometry
0.5	2.72
1	3.57
2	3.49
5	3.53
FAS, Co ₃ O ₄	2.44

The UV-visible spectra of all investigated samples are shown in Fig. 5.

As we can see by the figure, we have samples with absorbance bands and others with none at the region of 200–600 nm. This demonstrates the effect of Al³⁺ ion substitution by cobalt ones in all spinel structure samples and can obviously show electronic transition changes that can take place in the spinel structure. The spinel compositions of Co/Al molar ratio equal to 0.5 and 2 showed some absorption bands; the band at around 450 nm of Co/Al = 0.5 was shifted to 540 nm of Co/Al = 2, indicating the substitution effect. More notably, the samples of no absorption bands were observed for Co/Al molar ratio of 1 and 5 and also for the FAS one.

For more interpretation, the absorption of the samples containing Co/Al = 0.5 and 2 in the range from 540 to 630 nm can be attributed to the absorption of the colors yellow, orange, and red. Thus, the reflectance occurs in the complementary colors, namely violet, blue, and cyan, centered in the blue. The Co²⁺ ion present a 3d⁷ configuration and can occupy tetrahedral and octahedral sites in spinel-type structures. For such ions, there are, in the UV-vis region, three spin-allowed and three spin-forbidden electronic transitions, ascribed to ⁴A₂(F) → ⁴T₁(P) and ⁴A₂(F) → ²T(G), respectively [41, 42].

The absorption at approximately 550, 580, and 620 nm can be attributed to the spin-allowed ⁴A₂(F) → ⁴T₁(P) transition of the Co⁺² ions in tetrahedral sites.

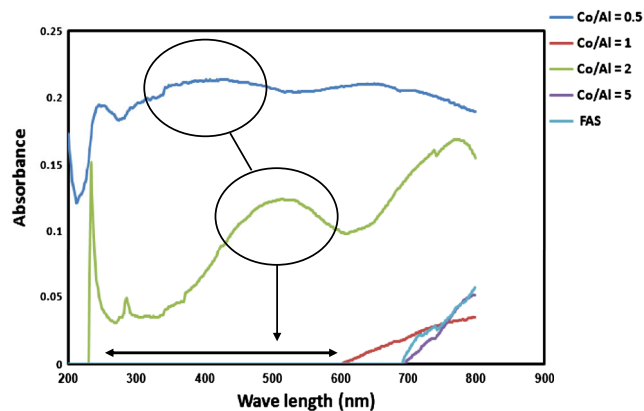


Fig. 5 UV-visible spectra of spinel cobalt aluminate structures containing different Co/Al molar ratios

Table 5 Colorimetric data of spinel cobalt aluminate structures containing different molar ratios (Co/Al)

Molar ratio, Co/Al	L^*	a^*	b^*
0.5	22.20	-4.32	-2.65
1	16.75	-0.69	-0.48
2	16.80	-1.43	-1.6
5	14.40	-0.97	-1.08
FAS, Co_3O_4	16.50	-0.60	-1.27

On the other hand, the absorption observed at around 478 nm is assumed to be related to spin-forbidden transitions reported by Zayat and Levy [42]. Zayat and Levy [42] reported that the absorption observed at 408, 447, and 479 nm are related to the spin-forbidden $^4A_2(F) \rightarrow ^2T(G)$ transition of the Co^{2+} ions in octahedral sites. On the other hand, Stangar et al. [41] considered that the bands whose wavelengths are below 520 nm are due to the electronic transitions of Co^{3+} in octahedral sites. Kim et al. [43] reported that the absorption around 752 nm is assigned to a $t_{2g}(\text{Co}^{3+}) \rightarrow t_2(\text{Co}^{2+})$ d–d charge transfer (CT) transition, from the $d(t_{2g})$ states of the octahedral Co^{3+} ion to the $d(t_2)$ states of the tetrahedral Co^{2+} ion. In addition, the ramp in the low wavelength part of the spectrum suggests the occurrence of charge transfer processes in these samples. The colorimetry analysis, L^* , a^* and b^* , values of all investigated spinel structure samples are shown in Table 5. The yield of blue color is mainly governed by the parameter b^* : The more b^* value increases in negative, the more intense blue color generates. On the other hand, the coordinate L^* gives the lightness of the color (the higher L^* , the lighter), also being an indirect measurement of brightness or intensity of the color (the lower L^* , the brighter or more intense the color). In general, the sample containing Co/Al molar ratio of

0.5 (CoAl_2O_4) showed high values of all colorimetric data compared to the other ones.

These colorimetric data change with the Co/Al molar ratio change, demonstrating the transition effect of cobalt ions from tetrahedral sites to octahedral ones in the spinel structure. The more interesting notice is that the samples of Co/Al molar ratio equal to 0.5 and 2 have the highest colorimetric values compared to the other ones. This comes in a good agreement with what observed before in UV-visible spectra part where the only same two samples showed absorption bands.

Figure 6 shows magnetization (M) versus applied magnetic field (H) at room temperature for the spinel structures. All values of magnetic property parameters are shown in Table 6. The absence of hysteresis loop on all samples is indicative of the presence of super paramagnetic and single-domain crystals [44]. If there is a little opening of a loop, this may be related to the uncompensated surface spin of the nanoparticles. To also approve the super paramagnetic behavior of the samples, experimentally ($\eta_B = MW \times M_s / 5585$) and theoretically ($\eta_B = M_B - M_A$) magnetic moments (η_B) of Co/Al = 1 sample as an example were calculated and found equal to 0.0020 and 0.0021 for the experimentally and theoretically ones, respectively. The very low values of magnetic moments represent the super paramagnetic feature of this sample. In contrast, the values of M_B and M_A were calculated according to the proposed cation distribution of the Co/Al = 1 sample (Table 3). The good matching of the two experimentally and theoretically values also confirms the accurate distribution of cobalt and aluminum in both octahedral and tetrahedral sites of the spinel.

Also, the saturation magnetization (M_s) varies with molar ratio (Co/Al) indicating the effect of ratio between cobalt and aluminum ions in the spinel structure on the magnetic properties. Here, it is a worthwhile to mention that the values of saturation magnetization (M_s) come in a good agreement with what was reported before in the part of oxygen content ratio,

Fig. 6 M-H curves of spinel cobalt aluminate structures containing different Co/Al molar ratios at room temperature

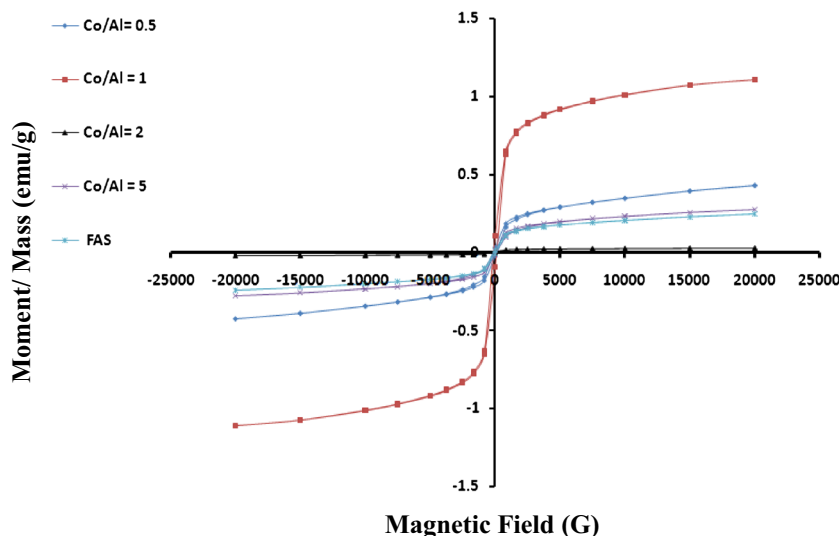


Table 6 Values of particle size, saturation magnetization (M_s), and coercivity (H_c) for spinel cobalt aluminate structures containing different molar ratios (Co/Al)

Molar ratio, Co/Al	Particle size (nm)	M_s (emu g ⁻¹)	H_c (G)
0.5	23	0.428	122.44
1	23	1.11	112.32
2	32	0.055	120.62
5	21	0.274	104.58
FAS, Co ₃ O ₄	25	0.243	84.67

where these values have the same trend. This can be interpreted as when the sample has a predominant Co³⁺ content, its saturation magnetization value will increase and the opposite is right. This also can be supported with a literature work concerning the magnetic moments of Co²⁺ and Co³⁺ [45, 46]. The authors reported that the magnetic moments of both Co²⁺ and Co³⁺ are 2.7 and 3.7 μ_B , respectively. At the same time and in general, the saturation magnetization values (M_s) also come in a good agreement with the particle size, where the particle size decrease enhances the saturation magnetization value and the opposite also is right. This enhancement can be attributed to a modification in the long-range cycloid spin structure of cobalt aluminate spinel [47]. The high optimum value of saturation magnetization ($M_s = 1.11$ emu g⁻¹) was observed for the spinel structure prepared with equal ratio of cobalt and aluminum ions (Co/Al = 1, Co₁Co_{0.5}Al_{1.5}O₄) and has a particle size of 23 nm. The magnetization values for the other samples come with the following order: [Co/Al = 0.5, CoAl₂O₄ > Co/Al = 5, Co₂Co_{0.5}Al_{0.5}O₄ > FAS, Co₃O₄ > Co/Al = 2, Co₂AlO₄].

We can conclude that there are two important factors affecting the magnetic properties of the spinel structures: particle size and molar ratio (which affect unit cell volume, density, and porosity). For every sample, there is a competition at the same time

between the two factors, which can be predominant and enhance the magnetization.

The two factors can affect with two important mechanisms; surface-driven effect is the enhancement of the magnetic anisotropy (K_{eff}) with decreasing particle size [48, 49]. In addition to the surface effect, the order–disorder characteristic of the samples has also a strong influence on the decrease of saturation magnetization [50]. For the sample having Co/Al = 1, the super paramagnetic behavior is characterized by higher saturation magnetization ($M_s = 1.11$ emu g⁻¹). The relatively higher saturation value may be due to the fact that the anisotropic features of these nanocrystals have enhanced dipole–dipole interaction [51].

To further show the good saturation magnetization value (M_s) of our sample, Co/Al = 1, Co₁Co_{0.5}Al_{1.5}O₄, a comparison was performed with recent previous CoAl₂O₄ materials prepared using different methods like what was studied by Chandradassa et al. [52] (CoAl₂O₄ prepared by reverse microemulsion process, $M_s = 0.23$ emu g⁻¹, particle size 57 nm).

Figure 7 shows the electrical properties (AC conductivity, frequency = 100 Hz) of all investigated samples at a temperature range of 298–343 K. From the figure, we can see that the sample containing Co/Al molar ratio equal to 0.5 has a minimum AC conductivity and the other one containing Co/Al molar ratio equal to 1 has a maximum ionic conductivity, the same sample of the highest saturation magnetization value (M_s , see Table 6). In the case of undoped CoAl₂O₄, hopping mechanism is considered responsible for the electrical conduction in which the hopping of holes takes place between the interstitial sites to occupy Al³⁺ and cobalt ions (Co²⁺) at the octahedral sites [53]. As Al³⁺ ions were substituted by cobalt ones (Co²⁺ and Co³⁺), this means that the system will have extra electrons, and as a result, all substituted spinels will show a high conductivity by the hopping mechanism (between Co²⁺ and Co³⁺ in octahedral site) compared to the sample of Co/Al = 0.5 (no substitution).

Also, since the spinel system contains a number of defects in the form of Co, Al, and O vacancies [54], which can affect more

Fig. 7 Temperature dependence of AC conductivity for spinel cobalt aluminate structures containing different Co/Al molar ratios at 100 Hz

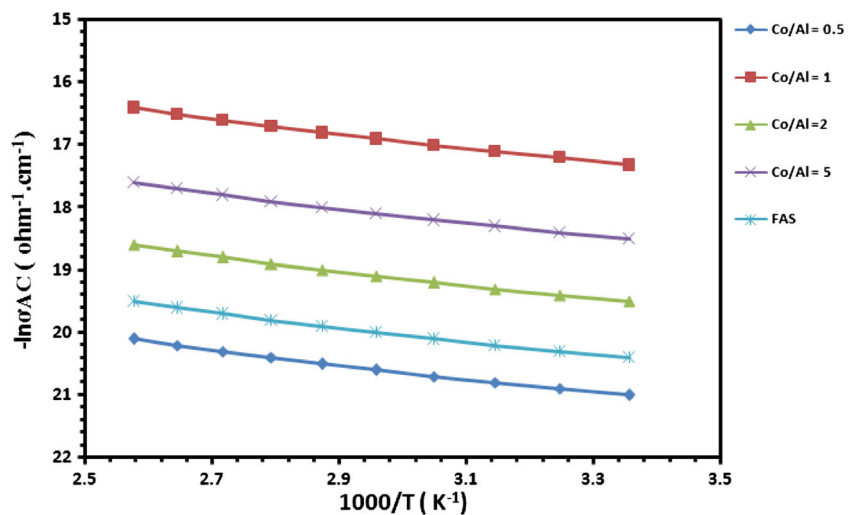


Table 7 Values of AC-conductivity and activation energy for spinel cobalt aluminate structures containing different molar ratios (Co/Al)

Molar ratio, Co/Al	AC conductivity at 298 K ($\Omega^{-1} \text{ cm}^{-1}$)	Activation energy (E_a , eV)
0.5	4.6×10^{-10}	0.15
1	3.1×10^{-8}	0.10
2	3.4×10^{-9}	0.13
5	9.2×10^{-9}	0.12
FAS, Co_3O_4	1.53×10^{-9}	0.14

the electrical properties [55–59], in addition to the expected oxide ion defect formation [this defect can be also approved by the oxygen content change in the spinels (see Table 4)], these defects produce local deformations in the system in addition to the local displacement in the direction of the local electrical field resulted in due to the electron hopping. Thus, a number of electrons together with the defects present in the system form small polarons. So, in addition to electron hopping, the hopping of the small polarons between the adjacent sites, i.e., tetrahedral and/or octahedral sites occupied by the cobalt and aluminum, also contributes to the conductivity. Also, the electrical conductivity increase with temperature increase mainly can be attributed to the thermally activated mobility of electrons and that of the small polarons, the hopping of which is enhanced by rise in temperature. More notably, the spinel samples did not show a regular trend to the conductivity increase. The AC conductivity order of all samples can be shown as

$$\left[\begin{aligned} \text{Co/Al} = 1, \text{CoCo}_{0.5}\text{Al}_{1.5}\text{O}_4 &> \text{Co/Al} \\ &= 5, \text{Co}_2\text{Co}_{0.5}\text{Al}_{0.5}\text{O}_4 > \text{Co/Al} \\ &= 2, \text{Co}_2\text{AlO}_4 > \text{FAS, Co}_3\text{O}_4 > \text{Co/Al} = 0.5, \text{CoAl}_2\text{O}_4 \end{aligned} \right]$$

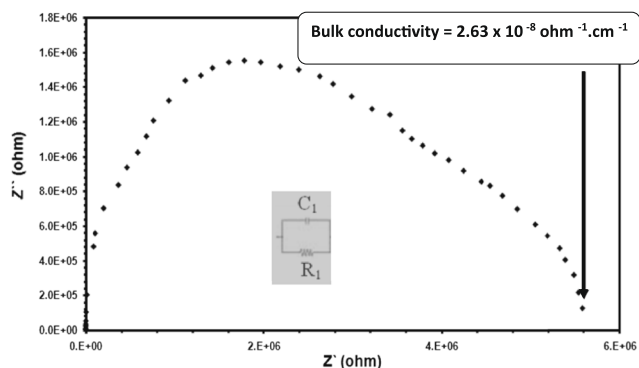


Fig. 8 Complex impedance for spinel cobalt aluminate structure containing Co/Al molar ratio of 1 ($\text{CoCo}_{0.5}\text{Al}_{1.5}\text{O}_4$) at room temperature (298 K)

All room temperature conductivity values and activation energies are shown in Table 7. As we can see, the activation energy values come in agreement order of the conductivity values to show that the maximum ionic conductivity sample has a value of 0.1 eV and that of minimum one has a value of 0.15 eV.

The complex impedance spectrum was also studied for the optimized sample of the high conductivity and saturation magnetization values (Fig. 8). The figure showed an impedance spectrum consisting of a semicircle. This semicircle is related to the electronic conduction process [60–67]. The value of bulk conductivity was calculated to equal $2.63 \times 10^{-8} \Omega^{-1} \text{ cm}^{-1}$ at room temperature. The equivalent circuit was also determined and shown in Fig. 8, where R_1 is the bulk resistance of the sample and C_1 is its bulk capacity.

To further investigate the morphology of the high conductivity and saturation magnetization (M_s) spinel sample, [Co/Al = 1, ($\text{CoCo}_{0.5}\text{Al}_{1.5}\text{O}_4$)], TEM was performed and showed a high agglomeration of nanorod particles (Fig. 9a), that was showed with high magnification in Fig. 9b.

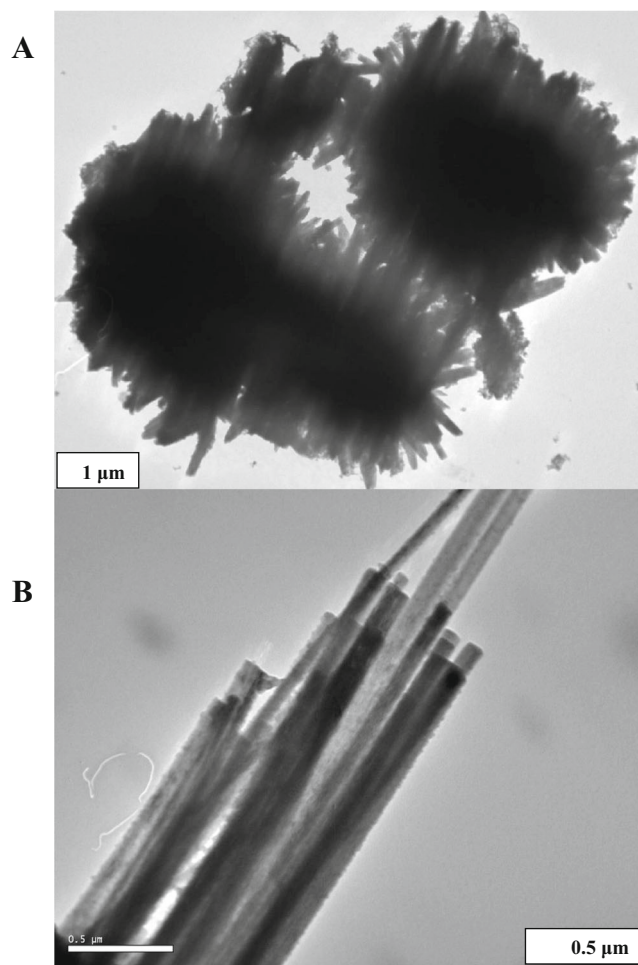


Fig. 9 a, b TEM micrographs of spinel cobalt aluminate structure containing Co/Al = 1, with two different magnifications

Conclusions

Aluminum substituted by cobalt of cobalt aluminates were successfully synthesized by the thermal decomposition to form the following spinel structures: CoAl_2O_4 , $\text{CoCo}_{0.5}\text{Al}_{1.5}\text{O}_4$, Co_2AlO_4 , $\text{Co}_2\text{Co}_{0.5}\text{Al}_{0.5}\text{O}_4$, and Co_3O_4 , respectively, with the following different molar ratios: Co/Al = 0.5, 1, 2, 5, and FAS (Co_3O_4), respectively. The Al^{3+} ions substituted by cobalt ones showed an obvious effect on the lattice parameter (a), porosity (p), and unit cell volume (V) of the spinel samples. The samples of Co/Al molar ratio equal to 0.5 and 2 have the highest colorimetric values compared to the other ones.

Two important factors affect the magnetic properties of the spinel structures: particle size and molar ratio (which affect unit cell volume, density, and porosity). For every sample, there is a competition at the same time between the two factors, which can be predominant and enhance the magnetization.

Also, the values of saturation magnetization (M_s) come in a good agreement with oxygen content ratio. This can be interpreted as when the sample has a predominant Co^{3+} content, its saturation magnetization value will increase and the opposite is right. The high value of saturation magnetization ($M_s = 1.11 \text{ emu g}^{-1}$) and conductivity ($3.1 \times 10^{-8} \Omega^{-1} \text{ cm}^{-1}$) was observed for the spinel structure prepared with equal ratio of cobalt and aluminum ions (Co/Al = 1, $\text{Co}_1\text{Co}_{0.5}\text{Al}_{1.5}\text{O}_4$). The value of bulk conductivity of the optimized spinel structure of cobalt aluminate was calculated to equal to $2.63 \times 10^{-8} \Omega^{-1} \text{ cm}^{-1}$ at room temperature.

At last, our optimized spinel sample of Co/Al = 1 showed a good saturation magnetization value when compared to a previous reported work studied by Chandradassa et al. (CoAl_2O_4 prepared by reverse microemulsion process, $M_s = 0.23 \text{ emu g}^{-1}$, particle size 57 nm), making the sample promising for the high-density magnetic recording and microwave device applications.

Acknowledgements The first author of this manuscript would like to thank the financial support of Benha University (<http://www.bu.edu.eg/en/>), Egypt, to complete this scientific work through a competitive research project (Third stage, Project N. 10.; code: 4/1/C).

References

- Reddy MV, Beichen Z, Jia'enNichollette L, Kaimeng Z, Chowdari BVR (2011) *Electrochemical and Solid State Letters* 14:A79
- Reddy MV, Kenrick KYH, Wei TY, Chowdari BVR (2011) *Journal of the Electrochemical Society* 158(12):A1423
- Reddy MV, Yu C, Jiahuan F, Lohand KP, Chowdari BVR (2012) *RSC Adv* 2:961
- Reddy MV, Xu Y, Rajarajan V, Ouyang T, Chowdari BVR (2015) *ACS Sustain Chem Eng* 3(12):3035–3042
- ShahulHameed A, Bahiraei H, Reddy MV, Shoushtari MZ, Vittal JJ, Ong CK, Chowdari BVR (2014) *ACS Appl Mater Interfaces* 6(13):10744
- Darbar D, Reddy MV, Sundarrajan S, Pattabiraman R, Ramakrishna S, Chowdari BVR (2016) *Mater Res Bull* 73:369
- Reddy MV, Quan CY, Teo KW, Ho LJ, Chowdari BVR (2015) *J Physical Chemistry C* 119(9):4709
- Bid S, Pradan SK (2003) *Mater Chem Phys* 82:27–37
- Ayala RE, Marsh DW (1991) *Ind Chem Res* 30:55–60
- Sepelak V, Bergmann I, Indris S, Feldhoff A, Hahn H, Becker KD, Grey CP, Heitjans P (2011) *J Mater Chem* 21:8332
- Lo Jacono M, Schiavello M, Cimino A (1971) *J Phys Chem* 75:1044
- Andrushkova OV, Ushakov VA, Polubojarov VA, Avvakumov EG (1992) *Sibirskii Khim Zh* 3:97
- Antolini E, Zhecheva E (1998) *Mater Lett* 35:380
- Baydi ME, Poillerat G, Rehspringer JL, Gautier JL, Koenig JF, Chartier P (1994) *J Solid-State Chem* 109:281
- Chemlal S, Larbot A, Persin M, Sarrazin J, Sghyar M, Rafiq M (2000) *Mater Res Bull* 35:2515
- Cho WS, Kakihana M (1999) *J Alloy Compd* 287:87
- Buxbaum G (1993) *Industrial inorganic pigments*, 1st edn. VCH, Weinheim, p 85
- Zayat M, Levy D (2002) *J Sol-Gel Sci Technol* 25:201–206
- Wang C, Bai X, Liu S, Liu L (2004) *J Mater Sci* 39:6191–6201
- Li W, Li J, Guo J (2003) *J Eur Ceram Soc* 23:2289–2295
- Mimani T, Alloys J (2001) *Compd*. 315:123–128
- Choa W-S, Kakihanab M, Alloys J (1999) *Compd* 287:87–90
- Wang C, Liu S, Liu L, Bai X (2006) *Mater Chem Phys* 96:361–370
- Chen Z-Z, Shi E-W, Li W-J, Zheng Y-Q, Zhuang J-Y, Xiao B, Tang L-A (2004) *MaterSci Eng B* 107:217–223
- Ouahdi N, Guillemet S, Durand B, El Ouatib R, Er Rakhob L, Moussab R, Samdi A (2008) *J Eur Ceram Soc* 28:1987–1994
- Guorong H, Xinrong D, Yanbing C, Zhongdong P (2007) *Rare Metals* 26:236–241
- Meyer F, Dierstein A, Beck C, Hlirtl W, Hempelmann R, Mathur S, Veith M (1999) *Nanostruct Mater* 12:71–74
- Meyer F, Hempelmann R, Mathur S, Veith M (1999) *J Mater Chem* 9:1755–1763
- Walsh A, Wei S-H, Yan Y, Al-Jassim MM, John A (2007) *Turner, PHYSICAL REVIEW B* 76:165119
- Mahmoud WE, El-Mallah H (2009) *J Phys D Appl Phys* 42:035502
- Chandradass J, Balasubramanian M, Kim KH (2010) *Alloys Compd* 506:395–399
- K. Nakamoto (1986), *Infrared and Raman Spectra of Inorganic and Coordination Compounds*, John Wiley & Sons, New York.
- B. Schrader (Ed.) (1995), *Infrared Raman spectroscopy: methods and applications*, VCH, Weinheim
- Farag ISA, Ahmad MA, Hammad SM, Moustafa AM (2001) *Egypt. J. Solids* 24:215
- Iqbal MJ, Farooq S (2007) *Mater Sci Eng B* 136:140
- Hong YS, Ho CM, Hsu HY, Liu CT (2004) *J Magn Magn Mater* 279:401
- Barakat MM, Henaish MA, Olofa SA, Tawfik A (1991) *J Therm Anal Calorim* 37:241
- Sattar AA (2004) *Egypt J Solids* 27:99
- Ahmed MA, Okasha N, Oaf M, Kershi RM (2007) *J Magn Magn Mater* 314:128
- Mohamed MB, Yehia M (2014) *Alloys Compd* 615:181–187
- Stangar UL, Orel B, Krajnc M (2003) *Journal of Sol-Gel Science and Technology* 26:771–775
- Zayat M, Levy D (2000) *Chem Mater* 12:2763–2769
- Kim KJ, Kim HK, Park YR, Ahn GY, Kim CS, Park JY (2006) *Hyperfine Interactions* 169:1363–1369
- Upadhyay T, Upadhyay RV, Mehta RV (1997) *Phys Rev B* 55:5585–5588

45. Suard E et al (2000) *phys RevJ* 61B:R11871
46. Fauth F et al (2001) *Eur Phys J* 21B:163
47. Wang J, Neaton JB, Zheng H, Nagarajan V, Ogale SB, Liu B, Viehland D, Vaithyanathan V, Schlom DG, Waghmare UV, Spaldin NA, Rabe KM, Wuttig M, Ramesh R (2003) *Science* 299:1719
48. Respaud M, Broto JM, Rakoto H, Fert AR, Thomas L, Barbara B, Verelst M, Snoeck E, Lecante P, Mosset A, Osuna J, Ould Ely T, Amiens C, Chaudret B (1998) *Phys Rev Lett* 57:2925–2935
49. Bodker F, Morup S, Linderorth S (1994) *Phys Rev Lett* 72:282–285
50. Kumar S, Singh V, Aggarwal S, Mandal UK, Kotnala RK *J Phys Chem C*. doi:10.1021/jp911586d
51. Yu D, Sun X, Zou J, Wang Z, Wang F, Tang K, *Phys J* (2006) *Chem B* 110:21667–21671
52. Chandradassa J, Balasubramanianb M, Kima KH (2010) *J of Alloys and Compounds* 506:395–399
53. Keer HV, Bodas MG, Bhaduri A, Biswas AB (1975) *J Inorg Nucl Chem* 37:1605
54. Ahmad J, QadeerAwan M, Mazhar ME, Ashiq MN (2011) *Physica B* 406:254–258
55. Liu L, Huang Y, Li Y, Wu M, Fang L, Hu C, Wang Y (2012) *Physica B* (407):136–139
56. Li Y, Liang F, Liu L, Huang Y, Hu C (2012) *Mater Sci Eng B* 177: 673–677
57. Sun X, Deng J, Liu L, Liu S, Shi D, Fang L, Elouadi B (2016) *Mater Res Bull* 73:437–445
58. Liu L, Elouadi B (2014) *J Mater Sci Mater Electron* (25):4058–4065
59. Shi LLD, Fan L, Chen J, Li G, Fang L, Elouadi B (2015) *J Mater Sci Mater Electron* 26:6592–6598
60. Masoud EM (2015) *Alloys Compd* 651:157–163
61. Masoud EM, Khairy M, Mousa MA (2013) *Alloys Compd* 569: 150–155
62. Masoud EM, Mousa MA (2015) *Ionics* 21:1095–1103
63. ElBellih AA, Bayoumy WA, Masoud EM, Mousa MA (2012) *BullKoreanSoc* 33(9):2949–2954
64. Masoud EM, Elbellih AA, Bayoumy WA, Mousa MA (2013) *Alloys Compd* 575:223–228
65. Masoud EM, El-Bellih A-A, Bayoumy WA, Mousa MA (2013) *Mater Res Bull* 48(3):1148–1154
66. Masoud EM (2016) *Polym Test* 56:65–73
67. Masoud EM, Hassan ME, Wahdaan SE, Elsayed SR, Elsayed SA (2016) *Polym Test* 56:277–286